

# Tiny-BioMoE: a Lightweight Embedding Model for Biosignal Analysis

Stefanos Gkikas

gkikas@ics.forth.gr

Foundation for Research &  
Technology-Hellas  
Heraklion, Greece

Ioannis Kyprakis

ikyprakis@ics.forth.gr

Foundation for Research &  
Technology-Hellas  
Heraklion, Greece

Manolis Tsiknakis

tsiknaki@ics.forth.gr

Foundation for Research &  
Technology-Hellas and Hellenic  
Mediterranean University  
Heraklion, Greece

## Abstract

Pain is a complex and pervasive condition that affects a significant portion of the population. Accurate and consistent assessment is essential for individuals suffering from pain, as well as for developing effective management strategies in a healthcare system. Automatic pain assessment systems enable continuous monitoring, support clinical decision-making, and help minimize patient distress while mitigating the risk of functional deterioration. Leveraging physiological signals offers objective and precise insights into a person's state, and their integration in a multimodal framework can further enhance system performance. This study has been submitted to the *Second Multimodal Sensing Grand Challenge for Next-Gen Pain Assessment (AI4PAIN)*. The proposed approach introduces *Tiny-BioMoE*, a lightweight pretrained embedding model for biosignal analysis. Trained on 4.4 million biosignal image representations and consisting of only 7.3 million parameters, it serves as an effective tool for extracting high-quality embeddings for downstream tasks. Extensive experiments involving electrodermal activity, blood volume pulse, respiratory signals, peripheral oxygen saturation, and their combinations highlight the model's effectiveness across diverse modalities in automatic pain recognition tasks. *The model's architecture (code) and weights are available at <https://github.com/GkikasStefanos/Tiny-BioMoE>.*

## CCS Concepts

- Applied computing → Health informatics.

## Keywords

Pain assessment, pain recognition, deep learning, multimodal, foundation model, data fusion

## ACM Reference Format:

Stefanos Gkikas, Ioannis Kyprakis, and Manolis Tsiknakis. 2025. Tiny-BioMoE: a Lightweight Embedding Model for Biosignal Analysis. In *Proceedings of October 13–17, 2025 (ICMI)*. ACM, New York, NY, USA, 10 pages. <https://doi.org/XXXXXXX.XXXXXXX>

---

Permission to make digital or hard copies of all or part of this work for personal or classroom use is granted without fee provided that copies are not made or distributed for profit or commercial advantage and that copies bear this notice and the full citation on the first page. Copyrights for components of this work owned by others than the author(s) must be honored. Abstracting with credit is permitted. To copy otherwise, or republish, to post on servers or to redistribute to lists, requires prior specific permission and/or a fee. Request permissions from [permissions@acm.org](mailto:permissions@acm.org).

ICMI,

© 2025 Copyright held by the owner/author(s). Publication rights licensed to ACM.

ACM ISBN 978-x-xxxx-xxxx-x/YYY/MM

<https://doi.org/XXXXXXX.XXXXXXX>

## 1 Introduction

Pain serves as a vital evolutionary mechanism, alerting the organism to potential harm or signaling the onset of illness, and plays a vital role in the body's defense system by helping maintain physiological integrity [56]. It is a subjective experience comprising multiple components, including nociceptive, sensory, affective, and cognitive dimensions [43]. Pain has been described as a “*Silent Public Health Epidemic*” [35], emphasizing its widespread yet often underestimated impact. In nursing literature, it is also referred to as “*the fifth vital sign*” [33], reflecting the need for its routine and systematic assessment alongside other vital signs. In addition, opioid analgesics are the most frequently prescribed treatment for pain management [36], yet they often lead to addiction and overdose [57]. Moreover, their side effects—such as lethargy, depression, anxiety, and nausea—significantly affect both workforce productivity and overall quality of life [5]. The inherent subjectivity and complexity of pain assessment have been identified as significant challenges in both research and clinical practice. For example, pain management often relies on patients' subjective reports, making it difficult to administer medication with precision. This lack of objective evaluation contributes significantly to the overprescription and overuse of pain medications [40]. Moreover, managing and assessing pain in patients with—or at risk of—medical instability presents significant clinical challenges, particularly when communication barriers are present [50]. Research highlights that pain in critically ill adults remains frequently under-managed. A significant limitation is the lack of structured, comprehensive tools for assessing pain and supporting clinical decision-making in these contexts [44]. Furthermore, cancer-related pain is highly prevalent, particularly in advanced stages of the disease, with its incidence exceeding 40% [3]. Additionally, the presence of negative emotions such as fear and sadness can influence pain expression, further complicating accurate assessment [58].

Precise evaluation and understanding of the factors influencing pain are crucial for achieving effective pain management [55]. Self-report methods, such as numerical rating scales and questionnaires, remain the gold standard for evaluating patient experiences. However, their reliability significantly diminishes in cases where patients exhibit altered consciousness, cognitive impairments, or communication difficulties [28]. Behavioral cues—such as facial expressions, vocalizations, and body movements—are widely used to infer pain, particularly in patients who cannot communicate [9]. Complementary to these, physiological signals like electrocardiography (ECG), electromyography (EMG), and electrodermal activity (EDA) provide deeper insights into the body's response to pain

[23]. Physiological signals play a crucial role in pain assessment by enabling a more objective and accurate understanding of a person’s condition. Sabbadini *et al.* [54] emphasized the importance of incorporating raw physiological data, such as continuous waveforms, to capture the intricate relationship between pain and physiological responses. Gozzi *et al.* [27] advocated for a broader perspective on pain as a multidimensional phenomenon, emphasizing the integration of physiological biomarkers with psychosocial factors.

This study introduces a lightweight embedding model, pretrained on over 4 million biosignals, and applies it to automatic pain assessment tasks across a wide range of modalities. Although numerous studies rely on biosignals, few models leverage large-scale pretraining. Moreover, given the growing concerns around the computational cost of large models for both training and inference, this work proposes a compact and efficient alternative, aiming to ensure accessibility regardless of the user’s hardware capabilities.

## 2 Related Work

Over the past decade, automatic pain assessment has gained increasing attention, with advancements shifting from conventional image and signal processing methods to more complex deep learning-based techniques [16]. The majority of existing methods are video-based, aiming to capture behavioral cues through facial expressions, body movements, or other visual indicators and employing a wide range of modeling strategies [4, 24, 25, 29]. While video-based approaches dominate the field, a considerable number of studies have also focused on biosignal-based methods, although to a lesser extent. These works have investigated the utility of various physiological signals, such as electrocardiography (ECG) [17, 18], electromyography (EMG) [46, 47, 59, 61], electrodermal activity (EDA) [1, 30, 41, 42, 48], and brain activity through functional near-infrared spectroscopy (fNIRS) [12, 13, 39, 52, 53]. For a more comprehensive analysis of biosignal modalities within automatic pain recognition frameworks, the reader is referred to [38].

In addition, multimodal approaches combining behavioral and physiological data have gained increasing attention in recent years, with several studies demonstrating the benefits of integrating multiple sources of information to improve performance. Many researchers explore combination of biosignals due to their potential to provide more accurate measurements. For instance, Jiang *et al.* [31] proposed a hybrid temporal-channel attention model that fuses ECG and galvanic skin response (GSR) signals, while in [32], the authors employed ECG and GSR signals alongside neural networks enhanced with Squeeze-and-Excitation blocks. Chu *et al.* [7] integrated blood volume pulse, ECG, and skin conductance level, using a hybrid approach that combined genetic algorithm-based feature selection with principal component analysis. On the other hand, Badura *et al.* [2] employed a multimodal setup in their effort to assess pain during physiotherapy, which included EDA, EMG, respiration, blood volume pulse (BVP), and hand force. Other researchers focus on combining physiological with behavioral modalities. The authors in [62] utilized facial videos in combination with ECG, EMG, and EDA, extracting a wide range of handcrafted features and fusing them. In [22], the authors combined facial videos and heart rate data to develop a transformer-based framework for recognizing pain intensity. Similarly, in [8], CNN and LSTM models

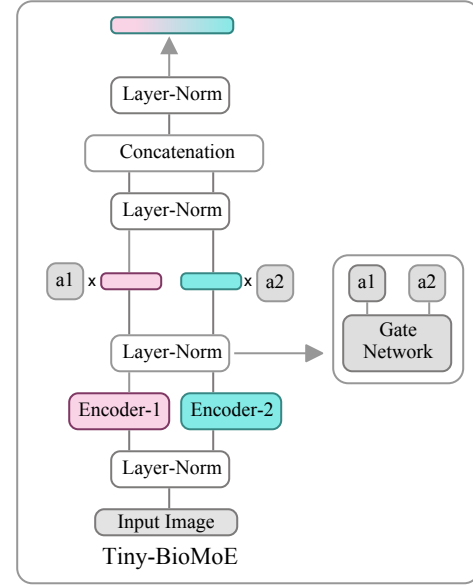


**Figure 1: Overview of the Tiny-BioMoE architecture.**

were used to analyze facial videos and EDA, achieving high performance. Finally, the authors in [21] proposed a foundation model that extracted feature representations from a wide range of modalities—both behavioral and physiological—for pain assessment.

## 3 Methodology

This section outlines the architecture of the proposed embedding model, the pretraining procedure, and the dataset used for pretraining. It also details the biosignal preprocessing steps and the transformation of these signals into visual representations. Additionally, it describes the augmentation and regularization techniques employed for the pain recognition tasks.

### 3.1 Tiny-BioMoE

Inspired by recent advancements in deep learning involving Mixture of Experts (MoE) architectures for language [6] and vision tasks [51], we propose *Tiny-BioMoE*—a lightweight MoE model comprising only 7.34 million parameters. The model consists of two vision transformer encoders, *Encoder-1* and *Encoder-2*. Both encoders process the input image independently to extract their respective embedding representations, which are subsequently fused into a unified feature vector. Table 2 reports the number of parameters and computational cost, measured in floating-point operations (FLOPs), while Figure 1 provides a high-level architectural overview.

**3.1.1 Encoder-1.** Integrates spectral and self-attention mechanisms in the initial layers, while relying exclusively on self-attention in the later stages. Each input image  $I$  is divided into  $n$  non-overlapping  $16 \times 16$  patches, reshaped into tokens  $\in \mathbb{R}^{n \times d}$  with  $d = 768$ , followed by positional encoding. To incorporate frequency information, a 2D Fast Fourier Transform (FFT) is applied to each token  $x$ , yielding  $X = \mathcal{F}[x] \in \mathbb{C}^{h \times w \times d}$ . A learnable complex-valued filter  $K \in \mathbb{C}^{h \times w \times d}$  modulates the spectral components via element-wise

multiplication:  $\tilde{X} = K \odot X$ . The filtered signal is then transformed back into the spatial domain using the inverse FFT:  $x \leftarrow \mathcal{F}^{-1}[\tilde{X}]$ . A depthwise convolution-based MLP enhances channel-wise interactions,  $f(x) = W_2 \cdot \text{GELU}(\text{DWConv}(W_1 \cdot x + b_1)) + b_2$ , with layer normalization applied before and after the FFT and IFFT. The attention layer employs standard scaled dot-product self-attention:

$$\tilde{X} = \text{Attn}(XW_q, XW_k, XW_v), \quad (1)$$

where  $W_q$ ,  $W_k$ , and  $W_v \in \mathbb{R}^{d \times d}$  are the projection matrices for queries, keys, and values, respectively. *Encoder-1* is composed of four hierarchical stages, each reducing spatial resolution by a factor of 2. The embedding dimensions across the stages are 64, 128, 320, and 96, with 1 attention head used per stage. Figure 2(a) illustrates the architecture of *Encoder-1*.

**3.1.2 Encoder-2.** Built upon hierarchical vision-transformer principles, incorporates mechanisms that enhance both efficiency and speed. *Encoder-2* consists of two core components: the *Spatial-Mixer* and the *Waterfall-Attention* module. The architecture is organized with *Waterfall-Attention* at its center, preceded and followed by *Spatial-Mixer* modules. The input image  $I$  is first divided into overlapping  $16 \times 16$  patches using a projection layer, with each patch embedded into a  $d$ -dimensional token. To capture local information, each patch  $T$  is processed with depth-wise convolution:

$$Y_c = K_c * T_c + b_c, \quad (2)$$

where  $T_c$  and  $Y_c$  are the input and output of channel  $c$ ,  $K_c$  is the channel-specific kernel, and  $b_c$  is the corresponding bias. Following convolution, batch normalization is applied as  $Z_c = \text{BN}(Y_c)$ , where BN denotes channel-wise normalization with learnable affine parameters. A feed-forward network (FFN) then facilitates inter-channel communication,  $\Phi^F(Z_c) = W_2 \cdot \text{ReLU}(W_1 \cdot Z_c + b_1) + b_2$ , where  $\Phi^F(Z_c)$  is the output of the feed-forward network for the input  $Z_c$ .  $W_1$  and  $W_2$  are the weight matrices of the first and second linear layers;  $b_1$  and  $b_2$  are the bias terms for the first and second linear layers, respectively, and ReLU is the activation function. Encoder-2 uses a single self-attention layer. For each input embedding,  $X_{i+1} = \Phi^A(X_i)$  is computed, where  $X_i$  is the full input embedding for the  $i$ -th block. The *Waterfall-Attention* module partitions the embedding into  $h$  segments, assigns each to a distinct head, and distributes the workload:

$$\tilde{X}_{ij} = \text{Attn}(X_{ij}W_{ij}^Q, X_{ij}W_{ij}^K, X_{ij}W_{ij}^V), \quad (3)$$

$$\tilde{X}_{i+1} = \text{Concat}[\tilde{X}_{ij}]_{j=1:h}W_i^P, \quad (4)$$

where each  $j$ -th head processes  $X_{ij}$ , the  $j$ -th segment of the full embedding  $X_i$ , structured as  $[X_{i1}, X_{i2}, \dots, X_{ih}]$ . Projection layers  $W_{ij}^Q$ ,  $W_{ij}^K$ , and  $W_{ij}^V$  map each segment into distinct subspaces, and  $W_i^P$  reunites the concatenated outputs. The waterfall design enriches each subsequent head by residual addition:  $X'_{ij} = X_{ij} + \tilde{X}_{i(j-1)}$ . Depth-wise convolution on every  $Q$  enables the self-attention to fuse global context with local cues. The model stacks three stages, each one a token layer deep. It halves the spatial resolution at every stage, progressively reducing the number of tokens. The associated embedding widths are  $d = 192, 288$ , and  $96$ , and the stages employ 3, 3, and 4 attention heads, respectively. Figure 2(b) illustrates the architecture of *Encoder-2*.

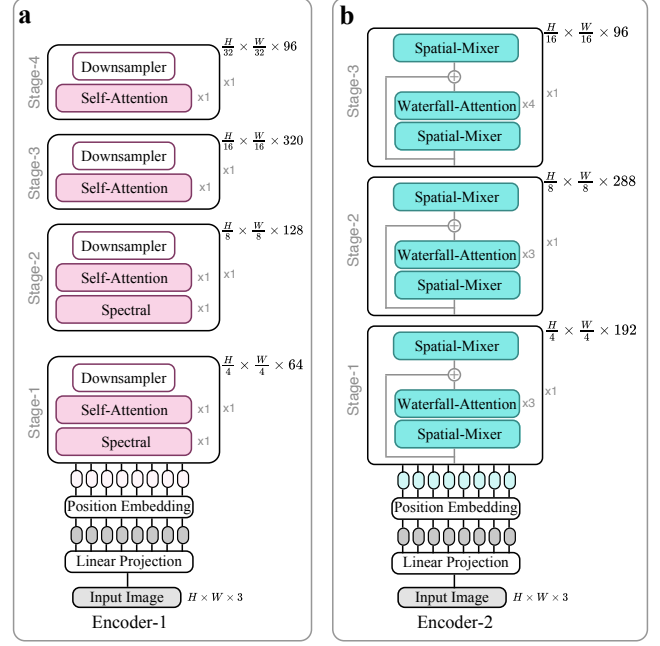


**Figure 2: Representation of the architecture of the main components of Tiny-BioMoE: (a) Encoder-1 and (b) Encoder-2.**

**3.1.3 Fusion.** Initially, a *LayerNorm* operation is applied to the input image tensor to ensure consistent normalisation before processing. The normalised input is then passed to both *Encoder-1* and *Encoder-2*, producing embeddings  $z_1$  and  $z_2$ , respectively. Each output is further normalised using a second *LayerNorm*, yielding  $\hat{z}_1$  and  $\hat{z}_2$ . A lightweight gating network is defined as:

$$g(x) = \text{HardTanh}(\text{ELU}(Wx)), \quad (5)$$

and produces per-channel modulation coefficients  $\alpha_1, \alpha_2 \in [0, 1]$ . These are applied element-wise to the encoder outputs:

$$z'_1 = \alpha_1 \odot \hat{z}_1, \quad z'_2 = \alpha_2 \odot \hat{z}_2. \quad (6)$$

Each encoder produces a 96-dimensional embedding, and after re-weighting and concatenation, the resulting feature vector becomes 192-dimensional:

$$z_{\text{cat}} = [z'_1 \parallel z'_2] \in \mathbb{R}^{192}. \quad (7)$$

A final *LayerNorm* is applied to  $z_{\text{cat}}$ , yielding the unified output used in downstream tasks.

### 3.2 Biosignal Pre-processing & Visualization

The biosignal samples used for both pretraining and pain-related tasks were converted into visual representations to enable compatibility with vision-based models. In total, six distinct transformations were applied: (1) Spectrogram-Angle plots encode the phase angle of the frequency components; (2) Spectrogram-Phase includes phase information with unwrapping applied to resolve discontinuities; (3) Spectrogram-PSD displays the power spectral density, reflecting how signal power varies across frequencies and time; (4) Recurrence plots map the recurrence of states in the signal's phase space to

**Table 1: Datasets utilized for the multitask learning-based pretraining process of the *PainFormer*.**

Dataset	Number of Samples	Modality
EEG-BST-SZ [14]	1.20M	EEG
Silent-EMG [15]	1.03M	EMG
ECG HBC Dataset [34]	2.16M	ECG
Total: 3 datasets–tasks	4.39M	

The reported number of samples refers exclusively to the training split, excluding validation and testing sets. Each sample in the corresponding dataset is represented by six distinct visualizations, as described in 3.2.

**Table 2: Number of parameters and FLOPS for the components of the proposed Tiny-BioMoE.**

Module	Parameters (M)	FLOPS (G)
Encoder-1	2.90	2.36
Encoder-2	4.13	0.68
Tiny-BioMoE	7.34	3.04

reveal temporal dynamics; (5) *Scalograms* represent time-frequency content using continuous wavelet transforms; (6) *Waveform* diagrams visualize the raw signal over time, capturing its amplitude, frequency, and phase characteristics. Figure 3 shows one example of each of these six visual representations. In addition, only the biosignals used in the pain-related tasks *i.e.*, electrodermal activity, blood volume pulse, respiratory signals, and peripheral oxygen saturation were filtered using a low-pass 5 Hz and band-pass filters of 0.04 – 1.7 Hz, 0.05 – 0.5 Hz, and 0.04 – 1.7 Hz, respectively.

### 3.3 Pretraining

*Tiny-BioMoE*, the proposed model, serves as an embedding extractor for biosignals. It was trained on 3 large-scale datasets comprising a total of 4.4 million samples—details are provided in Table 1. These datasets cover a wide range of biosignal modalities, including EEG, EMG, and ECG. The model was trained using a multi-task learning framework, where each dataset is considered as a distinct supervised task. All 14 tasks are learned jointly using the following objective:

$$L_{\text{total}} = \sum_{i=1}^3 [e^{w_i} L_{S_i} + w_i], \quad (8)$$

where  $L_{S_i}$  is the loss associated with the  $i$ -th task, and  $w_i$  are trainable weights that adaptively control each task’s contribution to the overall objective. Training was conducted for 200 epochs under this setup.

### 3.4 Augmentation Methods & Regularization

Several data augmentation techniques are applied during training for the pain recognition tasks. Every  $224 \times 224$  image undergoes a cascade of stochastic transformations. The *AugMix* method blends three randomly generated augmentation chains with the original

image, shifting a mixture of contrast, colour, and geometric perturbations to the image. In addition, *TrivialAugment* applies a single randomly chosen operation with a magnitude sampled uniformly. *Centre cropping* is applied with a probability drawn from a given range, where the crop size is selected randomly and the image is resized back to its original dimensions. Conditional *Gaussian blurring* applies noise by reducing high-frequency components. Two *Cutout* masks are applied—one placing a small number of blocks, the other covering the image with a higher number, both using blocks of equal size,  $32 \times 32$ . Beyond data-level augmentation, two stochastic regularizers have been utilized. A *Dropout* layer follows the encoder, with its keep probability gradually reduced linearly over training epochs:

$$p(t) = p_{\text{start}} + \frac{t}{T} (p_{\text{end}} - p_{\text{start}}), \quad 0 \leq t \leq T. \quad (9)$$

The cross-entropy loss employs a *Label-Smoothing* based on the same linear schedule, shifting from a soft target distribution toward one-hot labels. Finally, a cosine learning-rate profile with *Warmup* and *Coldown* schedules is also employed. All stochastic choices—operation selection, magnitudes, cropping ratios, mask locations, and probability draws—are resampled independently for every image at every batch. Throughout all experiments, the batch size is fixed to 32 and the learning rate is set to  $1e-4$ . Figure 4 presents an overview of the proposed multimodal pipeline.

## 4 Experimental Evaluation & Results

This study leverages the dataset released by the challenge organizers, which consists of electrodermal activity recordings from 65 participants. Data collection took place at the Human-Machine Interface Laboratory, University of Canberra, Australia, and is divided into 41 training, 12 validation, and 12 testing subjects. Pain stimulation was induced using transcutaneous electrical nerve stimulation (TENS) electrodes positioned on the inner forearm and the back of the right hand. Two pain levels were measured: pain threshold—the minimum stimulus intensity perceived as painful (low pain), and pain tolerance—the maximum intensity tolerated before becoming unbearable (high pain). The signals have a frequency of 100 Hz and a duration of approximately 10 seconds. We refer to [10] for a detailed description of the recording protocol and to [11] for information regarding the previous edition of the challenge. This study utilises all available modalities—EDA, BVP, respiratory signals, and peripheral oxygen saturation ( $\text{SpO}_2$ ). All experiments were conducted on the validation subset of the dataset and evaluated within a multi-class classification framework, encompassing three pain levels: No Pain, Low Pain, and High Pain. The validation results are reported in terms of macro-averaged accuracy, precision, and F1 score. The final results of the testing set are also reported. We note that all experiments followed a deterministic setup, eliminating the effect of random initializations; thus, any performance differences arose strictly from the chosen optimization settings, modalities, or other intentional changes rather than chance.

### 4.1 The Impact of Pretraining

The first series of experiments evaluates the impact of pretraining on model performance. All experiments followed a consistent training setup of 200 epochs. Table 3 reports the results obtained with the

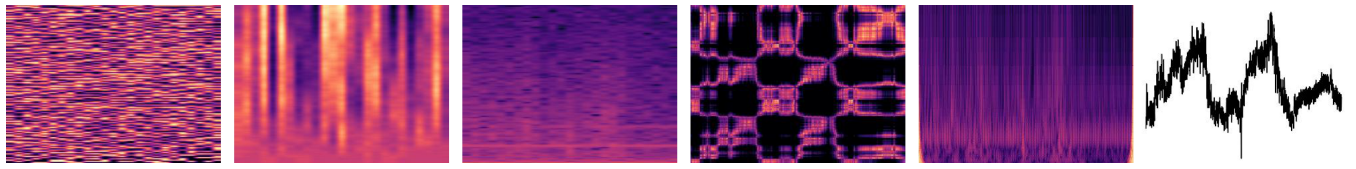


**Figure 3: Examples of the six visual representations used for biosignals. From left to right: Spectrogram-*Angle*, Spectrogram-*Phase*, Spectrogram-*PSD*, *Recurrence* plot, *Scalogram*, and *Waveform*.**

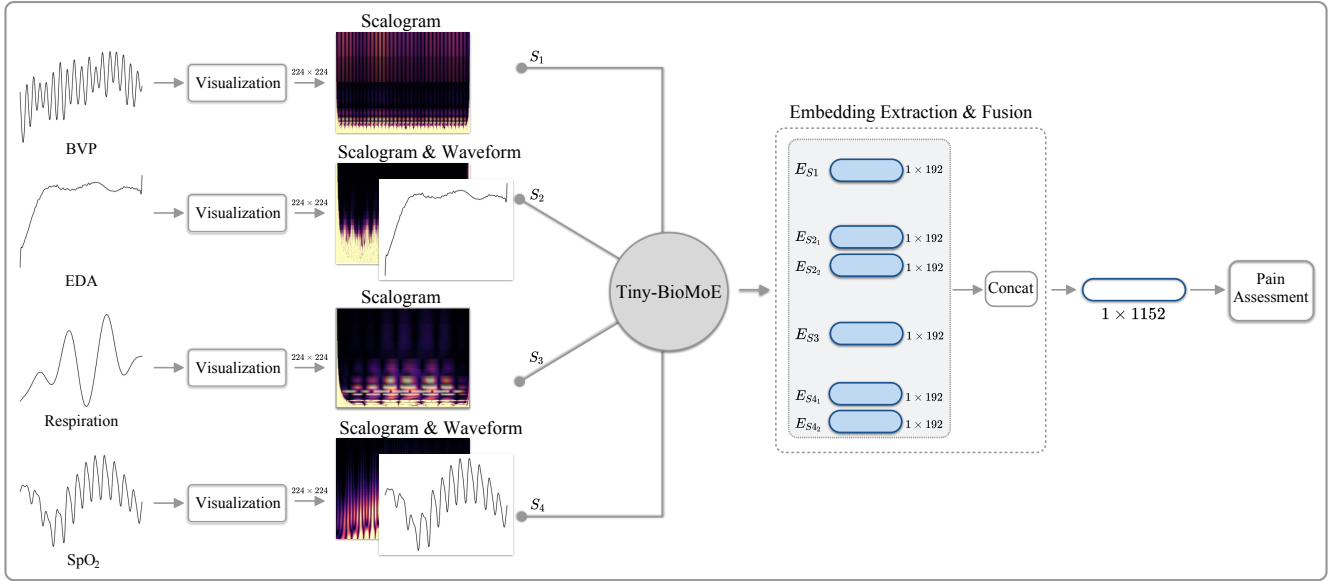


**Figure 4: Schematic overview of the proposed pipeline for pain assessment using various modalities and visual representation of them.**

*Tiny-BioMoE* model trained from scratch, retaining the same architecture but without pretraining. Table 4 shows the corresponding results using the pretrained version of *Tiny-BioMoE*, as described in Section 3.3, where the model acts as an embedding backbone. In all cases, the model was fine-tuned during training rather than kept frozen. For the BVP modality, training from scratch resulted in an accuracy of 45.24% with the *Angle* representation, 39.30% for *Phase*, and 42.58% for *PSD*. The *Recurrence* plot reached 42.09%, while the highest performance was achieved with the *Scalogram* at 66.53%. The *Waveform* also performed reasonably well with 42.90% accuracy. Using the pretrained model led to improvements across most representations. The most notable improvement was observed for *Recurrence*, which increased by over 5%, reaching 67.13%. In the case of EDA, overall performance was higher. With the scratch-trained model, *Angle* achieved 63.02%, and *Scalogram* reached 73.41%, again emerging as the top representation. Surprisingly, pretraining led to a slight decrease in performance: 61.36% for *Angle* and 71.15% for *Scalogram*. Notably, *PSD* achieved a precision of 80.60%, one of the highest observed. Respiration signals also showed strong results, with 45.61% for *Angle* and 71.91% for *Scalogram*. The pretrained model yielded minor fluctuations, with *Scalogram* improving to

73.53% and *Angle* slightly dropping to 44.78%. For the SpO<sub>2</sub> modality, pretraining resulted in consistent improvements across nearly all representations. *Angle* rose from 51.59% to 55.80%, *Phase* from 48.12% to 52.19%, and *PSD* from 47.86% to 54.97%. The most substantial gains were observed for *Recurrence* and *Waveform*, which increased by 13.46% and 15.62%, respectively. The only exception was *Scalogram*, which slightly decreased to 74.31%. Overall, the average accuracy across all representations and modalities increased from 52.13% with the scratch-trained model to 53.96% with the pretrained one. The most significant improvement occurred in the SpO<sub>2</sub> modality, where the average accuracy rose from 55.59% to 62.73%. Note that all the following experiments report results using the pretrained version of *Tiny-BioMoE*.

## 4.2 Fusion of Representations

The next series of experiments focuses on the fusion of representations within each modality. As previously discussed, each biosignal modality includes six distinct visual representations; however, not all contribute equally to performance. The goal is to evaluate which combinations of these representations can enhance the results. Fusion is performed by first extracting embeddings for each representation using the pretrained *Tiny-BioMoE*, followed by applying

**Table 3: Comparison of performance across different modalities and representations without pretraining (scratch).**

Modality	Representation	Task-MC		
		Accuracy	Precision	F1
BVP	Angle	<u>45.24</u>	49.42	<u>46.72</u>
BVP	Phase	39.30	<u>61.30</u>	40.48
BVP	PSD	42.58	58.24	45.03
BVP	Recurrence	42.09	45.95	43.47
BVP	Scalogram	<b>66.53</b>	<b>67.33</b>	<b>66.41</b>
BVP	Waveform	42.90	43.71	41.86
EDA	Angle	<u>63.02</u>	<u>69.12</u>	<u>64.83</u>
EDA	Phase	53.94	58.26	53.21
EDA	PSD	53.06	43.17	47.06
EDA	Recurrence	59.37	63.27	61.11
EDA	Scalogram	<b>73.41</b>	<b>73.59</b>	<b>73.03</b>
EDA	Waveform	61.48	68.32	63.45
Resp	Angle	<u>45.61</u>	51.85	45.57
Resp	Phase	<u>40.96</u>	45.11	42.85
Resp	PSD	43.42	<u>57.49</u>	<u>46.08</u>
Resp	Recurrence	36.16	39.08	36.22
Resp	Scalogram	<b>71.91</b>	<b>71.89</b>	<b>71.72</b>
Resp	Waveform	36.62	40.20	32.90
SpO <sub>2</sub>	Angle	51.59	58.85	53.76
SpO <sub>2</sub>	Phase	48.12	<u>72.53</u>	51.26
SpO <sub>2</sub>	PSD	47.86	67.33	50.23
SpO <sub>2</sub>	Recurrence	<u>55.18</u>	59.81	<u>57.06</u>
SpO <sub>2</sub>	Scalogram	<b>75.93</b>	<b>77.24</b>	<b>75.63</b>
SpO <sub>2</sub>	Waveform	54.87	59.74	56.03

two fusion methods: element-wise addition and concatenation. Two main strategies are examined: (i) fusion of all six representations for each modality, and (ii) fusion of the two top-performing representations per modality. The results are presented in Table 5. For the BVP modality, fusion of all six representations using addition yielded an accuracy of 54.01%, while concatenation improved the performance to 58.87%, the highest recorded for this modality. In contrast, fusion of only the *Scalogram* and *Recurrence* representations resulted in lower accuracy: 53.08% with addition and 49.18% with concatenation. In all cases, fusion led to decreased performance compared to using only the *Scalogram*, the best standalone representation for BVP. Regarding the EDA modality, fusion of all representations decreased accuracy to 67.75% with addition and 63.62% with concatenation. However, when only *Scalogram* and *Recurrence* were fused, accuracy improved to 76.85% and 77.88% respectively—both outperforming the best individual representation for this modality. A similar trend was observed in the respiration signals. Fusion of all representations via concatenation resulted in 69.87%, which was lower than the 73.53% achieved using only the *Scalogram*. Finally, for the SpO<sub>2</sub> modality, fusion of all six representations did not improve performance. However, fusing *Scalogram* and *Recurrence*

**Table 4: Comparison of performance across different modalities and representations with the pretrained model.**

Modality	Representation	Task-MC		
		Accuracy	Precision	F1
BVP	Angle	46.06	49.71	47.40
BVP	Phase	40.39	44.43	41.44
BVP	PSD	43.04	48.00	44.42
BVP	Recurrence	<u>47.43</u>	49.80	<u>48.26</u>
BVP	Scalogram	<b>67.13</b>	<b>65.42</b>	<b>62.19</b>
BVP	Waveform	43.67	<u>51.28</u>	44.00
EDA	Angle	61.36	63.19	61.85
EDA	Phase	51.29	58.22	53.87
EDA	PSD	52.57	<b>80.60</b>	50.82
EDA	Recurrence	55.48	57.05	56.22
EDA	Scalogram	<b>71.15</b>	<u>71.83</u>	<b>69.98</b>
EDA	Waveform	<u>63.46</u>	61.16	<u>62.00</u>
Resp	Angle	44.78	45.80	45.19
Resp	Phase	40.47	46.28	41.73
Resp	PSD	<u>45.29</u>	<u>51.40</u>	<u>46.18</u>
Resp	Recurrence	38.18	39.12	38.47
Resp	Scalogram	<b>73.53</b>	<b>73.93</b>	<b>73.40</b>
Resp	Waveform	33.33	26.78	29.70
SpO <sub>2</sub>	Angle	55.80	58.72	56.15
SpO <sub>2</sub>	Phase	52.19	56.37	53.65
SpO <sub>2</sub>	PSD	54.97	61.29	57.14
SpO <sub>2</sub>	Recurrence	68.64	70.45	69.18
SpO <sub>2</sub>	Scalogram	<b>74.31</b>	<b>74.37</b>	<b>74.25</b>
SpO <sub>2</sub>	Waveform	<u>70.49</u>	<u>71.66</u>	<u>71.03</u>

via concatenation led to an accuracy of 74.54%, showing a slight improvement over the best single-representation result.

### 4.3 Fusion of Modalities

The final experiments investigate the fusion of modalities along with their corresponding representations. Initially, the best performing representation for each modality is selected and fused using both addition and concatenation methods, as in previous experiments. Additionally, a configuration using only the *Scalogram* representation from each modality is examined, since it generally yields the highest individual performance. The results are shown in Table 6. Specifically, the selected configuration includes the *Scalogram* for BVP, the *Scalogram* and *Waveform* for EDA, the *Scalogram* for respiration, and the *Scalogram* and *Waveform* for SpO<sub>2</sub>. This fusion setup resulted in high performance, achieving 81.02% accuracy with addition and 82.41% with concatenation—the highest scores reported in this study. Using only the *Scalogram* from each modality for fusion did not further improve performance, but still yielded strong results, with both fusion methods reaching an accuracy of 74.77%. Figure 5 visualizes the accuracy performance across individual modality representations, fused representations, and multimodal combinations reported in this study.

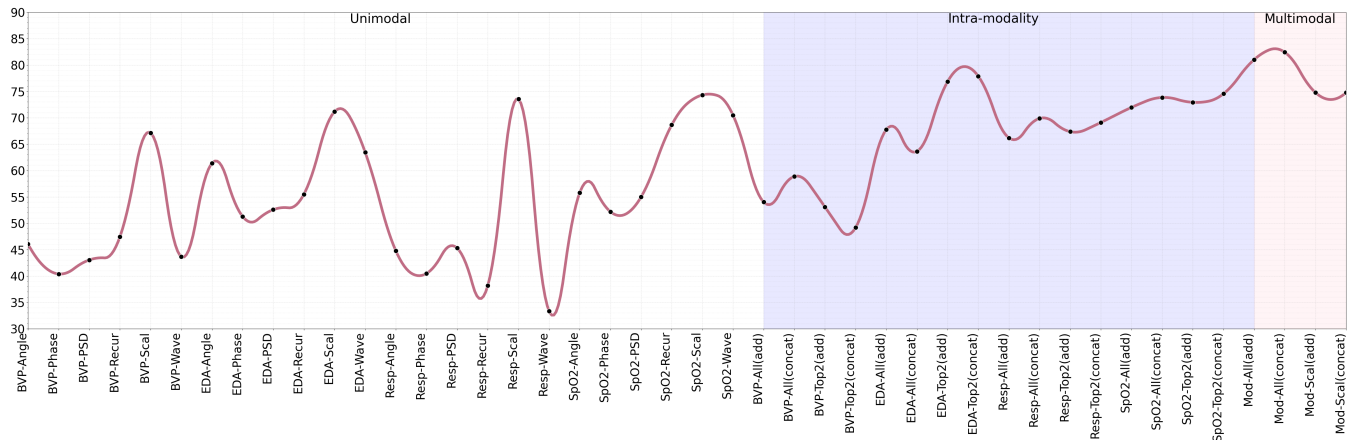


**Figure 5: Performance across modality representations, combinations of representations, and combinations of modalities.**

## 5 Comparison with Existing Methods

In this section, the proposed approach is compared with previous studies using the testing set of the *AI4PAIN* dataset. Some of these studies were conducted as part of the *First Multimodal Sensing Grand Challenge*. In contrast, others, including the present work, utilized data from the *Second Multimodal Sensing Grand Challenge*. The key distinction between the two challenges lies in the set of available modalities. Studies employing facial video or fNIRS have reported strong results, with accuracies of 49.00% by [49] and 55.00% by [45], respectively. Combining these two modalities also yielded competitive results, although not substantially better than using each modality alone. For instance, [60] reported 51.33%, and [21] achieved 55.69% using fused video and fNIRS data. Regarding the physiological modalities available in the *Second Grand Challenge*, some approaches achieved notably high performance, while others produced more limited results. In [20], an accuracy of 55.17% was reported using EDA in isolation, whereas [19] achieved 42.17% using only the respiration signal. The proposed method, which combines all available modalities—EDA, BVP, respiration, and SpO<sub>2</sub>—and utilizes specific visual representations for each, achieved an accuracy of 54.89%. This ranks among the highest performances reported on the dataset.

## 6 Conclusion

This study presents our contribution to the *Second Multimodal Sensing Grand Challenge for Next-Generation Pain Assessment (AI4PAIN)*, where all available modalities—EDA, BVP, respiration, and SpO<sub>2</sub>—were utilized. We introduced *Tiny-BioMoE*, a lightweight embedding model for biosignal analysis. With only 7.3 million parameters, a computational cost of 3.04 GFLOPs, and pretrained on 4.4 million biosignal-based representations, it serves as an efficient and versatile solution for a wide range of physiology-related tasks. Evaluated on the *AI4PAIN* dataset for pain recognition, *Tiny-BioMoE* demonstrated strong performance across modalities. A variety of visual representations were also explored. Results showed that the pretrained version of *Tiny-BioMoE* consistently outperformed its

non-pretrained counterpart, especially in cases where the individual modality alone had limited discriminative power. This is particularly important, as it enables the use of modalities that might otherwise be disregarded. A comprehensive set of experiments revealed a clear trend in performance, progressing from isolated representations to intra-modality fusion and ultimately to multimodal combinations. The highest accuracy was achieved through a multimodal approach, combining all four modalities and selected visual representations. We argue that small, efficient pretrained models, such as *Tiny-BioMoE*, are highly valuable and that future efforts should prioritize their development and open distribution to help democratize access to advanced physiological modeling, regardless of hardware constraints.

## Safe and Responsible Innovation Statement

This work relied on the *AI4PAIN* dataset [10, 11], made available by the challenge organizers, to assess automatic pain recognition methods. All participants confirmed the absence of neurological or psychiatric conditions, unstable health issues, chronic pain, or regular medication use during the session. Before the experiment, participants were thoroughly informed of the procedures, and written consent was obtained. The original study's human-subject protocol received ethical clearance from the University of Canberra's Human Ethics Committee (*approval number: 11837*). The proposed method was developed for continuous pain monitoring, aiming to enhance pain assessment protocols and improve patient care. However, as validation and testing were performed on controlled laboratory data, its deployment in real-world clinical settings requires further investigation and comprehensive evaluation.

## References

- [1] Sumair Aziz, Calvin Joseph, Niraj Hirachan, Luke Murtagh, Girija Chetty, Roland Goecke, and Raul Fernandez-Rojas. 2025. A two-stage architecture for identifying and locating the source of pain using novel multi-domain binary patterns of EDA. *Biomedical Signal Processing and Control* 104 (2025), 107454. <https://doi.org/10.1016/j.bspc.2024.107454>
- [2] Aleksandra Badura, Aleksandra Maslowska, Andrzej Myśliwiec, and Ewa Pietka. 2021. Multimodal Signal Analysis for Pain Recognition in Physiotherapy Using Wavelet Scattering Transform. *Sensors* 21, 4 (2021). <https://doi.org/10.3390/s21041311>

**Table 5: Comparison of performance across different fusion methods of representations.**

Modality	Representation	Fusion	Task-MC		
			Accuracy	Precision	F1
BVP	Scal, Recur, Angle, Wave PSD, Phase	add	<u>54.01</u>	<u>61.22</u>	<u>56.62</u>
	Scal, Recur, Angle, Wave PSD, Phase	concat	<b>58.87</b>	<b>63.40</b>	<b>60.18</b>
	Scal, Recur Scal, Recur	add	53.08	54.20	53.06
BVP	Scal, Recur Scal, Recur	concat	49.18	61.13	53.28
EDA	Scal, Wave, Angle, Recur PSD, Phase	add	67.75	68.01	64.63
	Scal, Wave, Angle, Recur PSD, Phase	concat	63.62	61.59	61.64
	Scal, Recur Scal, Recur	add	<u>76.85</u>	<u>73.70</u>	<u>75.06</u>
EDA	Scal, Recur Scal, Recur	concat	<b>77.88</b>	<b>76.34</b>	<b>76.88</b>
Resp	Scal, PSD, Angle, Phase Recur, Wave	add	66.18	<u>70.30</u>	65.27
	Scal, PSD, Angle, Phase Recur, Wave	concat	<b>69.87</b>	67.91	<u>68.81</u>
	Scal, PSD Scal, PSD	add	67.36	<b>71.34</b>	64.90
Resp	Scal, PSD Scal, PSD	concat	<u>69.10</u>	69.90	<b>69.17</b>
SpO <sub>2</sub>	Scal, Wave, Recur, Angle PSD, Phase	add	71.96	<u>74.59</u>	72.84
	Scal, Wave, Recur, Angle PSD, Phase	concat	<u>73.84</u>	74.11	<u>73.79</u>
	Scal, Recur Scal, Recur	add	72.92	72.93	72.90
SpO <sub>2</sub>	Scal, Recur Scal, Recur	concat	<b>74.54</b>	<b>74.95</b>	<b>74.22</b>

[3] Yeong Hak Bang, Yoon Ho Choi, Mincheol Park, Soo-Yong Shin, and Seok Jin Kim. 2023. Clinical relevance of deep learning models in predicting the onset timing of cancer pain exacerbation. *Scientific Reports* 13, 1 (2023), 11501.

[4] Ghazal Barghshady, Calvin Joseph, Niraj Hirachan, Roland Goecke, and Raul Fernandez Rojas. 2024. Acute Pain Recognition from Facial Expression Videos using Vision Transformers. In *2024 46th Annual International Conference of the IEEE Engineering in Medicine and Biology Society (EMBC)*. 1–4. <https://doi.org/10.1109/EMBC53108.2024.10781616>

[5] Ramin Benyamin, Andrea M Trescot, Sukdeb Datta, Ricardo M Buenaventura, Rajive Adlaka, Nalini Sehgal, Scott E Glaser, and Ricardo Vallejo. 2008. Opioid complications and side effects. *Pain physician* 11, 2S (2008), S105.

[6] Weilin Cai, Juyong Jiang, Fan Wang, Jing Tang, Sunghun Kim, and Jiayi Huang. 2025. A survey on mixture of experts in large language models. *IEEE Transactions on Knowledge and Data Engineering* (2025).

[7] Yaqi Chu, Xingang Zhao, Jianda Han, and Yang Su. 2017. Physiological Signal-Based Method for Measurement of Pain Intensity. *Frontiers in Neuroscience* Volume 11 - 2017 (2017). <https://doi.org/10.3389/fnins.2017.00279>

[8] Jaleh Farmani, Alessandro Giuseppi, Ghazal Barghshady, and Raul Fernandez Rojas. 2025. Multimodal Automatic Acute Pain Recognition Using Facial Expressions

**Table 6: Comparison of performance across different fusion methods of modalities.**

Modality	Representation	Fusion	Task-MC		
			Accuracy	Precision	F1
BVP	Scalogram				
	Scal, Wave	add	<u>81.02</u>	<u>81.72</u>	<u>81.36</u>
	Scalogram				
EDA	Scal, Wave	concat	<b>82.41</b>	<b>84.25</b>	<b>82.43</b>
	Scalogram				
	Scal, Wave				
Resp	Scalogram				
	Scal, Wave	add	74.77	75.47	74.84
	Scalogram				
SpO <sub>2</sub>	Scalogram				
	Scal, Wave	concat	74.77	75.75	75.23
	Scalogram				

**Table 7: Comparison of studies on the testing set of the AI4Pain dataset.**

Study	Modality	ML	Acc (%)
[37] <sup>†</sup>	fnIRS	ENS	53.66
[45] <sup>†</sup>	fnIRS	Transformer	55.00
[49] <sup>†</sup>	Video	2D CNN	49.00
[26] <sup>†</sup>	Video, fnIRS	Transformer	46.67
[60] <sup>†</sup>	Video, fNIRS	CNN-Transformer	51.33
[21] <sup>†</sup>	Video, fNIRS	Transformer	55.69
[20] <sup>‡</sup>	EDA	Transformer	55.17
[19] <sup>‡</sup>	Respiration	Transformer	42.24
Our <sup>‡</sup>	EDA, BVP, Resp, SpO <sub>2</sub>	MoE	54.89

ENS: Ensemble Classifier <sup>†</sup>: AI4PAIN-First Multimodal Sensing Grand Challenge <sup>‡</sup>: AI4PAIN-Second Multimodal Sensing Grand Challenge

and Physiological Signals. In *Neural Information Processing*, Mufti Mahmud, Maryam Doborjeh, Kevin Wong, Andrew Chi Leung, Zohreh Doborjeh, and M. Tanveer (Eds.). Springer Nature Singapore, Singapore, 49–62.

[9] Raul Fernandez Rojas, Nicholas Brown, Gordon Waddington, and Roland Goecke. 2023. A systematic review of neurophysiological sensing for the assessment of acute pain. *NPJ Digital Medicine* 6, 1 (2023), 76. <https://doi.org/10.1038/s41746-023-00810-1>

[10] Raul Fernandez Rojas, Niraj Hirachan, Nicholas Brown, Gordon Waddington, Luke Murtagh, Ben Seymour, and Roland Goecke. 2023. Multimodal physiological sensing for the assessment of acute pain. *Frontiers in Pain Research* 4 (2023). <https://doi.org/10.3389/fpain.2023.1150264>

[11] Raul Fernandez Rojas, Niraj Hirachan, Calvin Joseph, Ben Seymour, and Roland Goecke. 2024. The AI4Pain Grand Challenge 2024: Advancing Pain Assessment with Multimodal fNIRS and Facial Video Analysis. In *2024 12th International Conference on Affective Computing and Intelligent Interaction*. IEEE.

[12] Raul Fernandez Rojas, Calvin Joseph, Ghazal Bargshady, and Keng-Liang Ou. 2024. Empirical comparison of deep learning models for fNIRS pain decoding. *Frontiers in Neuroinformatics* (2024). <https://doi.org/10.3389/fninf.2024.1320189>

[13] Raul Fernandez Rojas, Mingyu Liao, Julio Romero, Xu Huang, and Keng-Liang Ou. 2019. Cortical Network Response to Acupuncture and the Effect of the Hegu Point: An fNIRS Study. *Sensors* 19, 2 (2019). <https://doi.org/10.3390/s19020394>

[14] Judith M. Ford, Vanessa A. Palzes, Brian J. Roach, and Daniel H. Mathalon. 2013. Did I Do That? Abnormal Predictive Processes in Schizophrenia When Button Pressing to Deliver a Tone. *Schizophrenia Bulletin* 40, 4 (07 2013), 804–812. <https://doi.org/10.1093/schbul/sbt072>

[15] David Gaddy and Dan Klein. 2020. Digital Voicing of Silent Speech. In *Proceedings of the 2020 Conference on Empirical Methods in Natural Language Processing (EMNLP)*. Association for Computational Linguistics, Online, 5521–5530. <https://doi.org/10.18653/v1/2020.emnlp-main.445>

[16] Stefanos Gkikas. 2025. A Pain Assessment Framework based on multimodal data and Deep Machine Learning methods. arXiv:2505.05396 [cs.AI] <https://arxiv.org/abs/2505.05396> arXiv preprint arXiv:2505.05396.

[17] Stefanos Gkikas., Chariklia Chatzaki., Elisavet Pavlidou., Foteini Verigou., Kyriakos Kalkanis., and Manolis Tsiknakis. 2022. Automatic Pain Intensity Estimation based on Electrocardiogram and Demographic Factors. *Proceedings of the 8th International Conference on Information and Communication Technologies for Ageing Well and e-Health - ICT4AWE*, 155–162. <https://doi.org/10.5220/001971700003188>

[18] Stefanos Gkikas, Chariklia Chatzaki, and Manolis Tsiknakis. 2023. Multi-task Neural Networks for Pain Intensity Estimation Using Electrocardiogram and Demographic Factors. In *Information and Communication Technologies for Ageing Well and e-Health*. Springer Nature Switzerland, 324–337. [https://doi.org/10.1007/978-3-031-37496-8\\_17](https://doi.org/10.1007/978-3-031-37496-8_17)

[19] Stefanos Gkikas, Ioannis Kyprakis, and Manolis Tsiknakis. 2025. Efficient Pain Recognition via Respiration Signals: A Single Cross-Attention Transformer Multi-Window Fusion Pipeline. arXiv:2507.21886 [cs.AI]

[20] Stefanos Gkikas, Ioannis Kyprakis, and Manolis Tsiknakis. 2025. Multi-Representation Diagrams for Pain Recognition: Integrating Various Electrodermal Activity Signals into a Single Image. arXiv:2507.21881 [cs.AI]

[21] Stefanos Gkikas, Raul Fernandez Rojas, and Manolis Tsiknakis. 2025. PainFormer: a Vision Foundation Model for Automatic Pain Assessment. arXiv:2505.01571 [cs.CV] <https://arxiv.org/abs/2505.01571>

[22] Stefanos Gkikas, Nikolaos S. Tachos, Stelios Andreadis, Vasileios C. Pezoulas, Dimitrios Zaridis, George Gkois, Anastasia Matomaki, Thanos G. Stavropoulos, and Dimitrios I. Fotiadis. 2024. Multimodal automatic assessment of acute pain through facial videos and heart rate signals utilizing transformer-based architectures. *Frontiers in Pain Research* 5 (2024). <https://doi.org/10.3389/fpain.2024.1372814>

[23] Stefanos Gkikas and Manolis Tsiknakis. 2023. Automatic assessment of pain based on deep learning methods: A systematic review. *Computer Methods and Programs in Biomedicine* 231 (2023), 107365. <https://doi.org/10.1016/j.cmpb.2023.107365>

[24] Stefanos Gkikas and Manolis Tsiknakis. 2023. A Full Transformer-based Framework for Automatic Pain Estimation using Videos. In *2023 45th Annual International Conference of the IEEE Engineering in Medicine & Biology Society (EMBC)*. 1–6. <https://doi.org/10.1109/EMBC40787.2023.10340872>

[25] Stefanos Gkikas and Manolis Tsiknakis. 2024. Synthetic Thermal and RGB Videos for Automatic Pain Assessment Utilizing a Vision-MLP Architecture. In *2024 12th International Conference on Affective Computing and Intelligent Interaction Workshops and Demos (ACIIW)*. 4–12. <https://doi.org/10.1109/ACIIW63320.2024.00006>

[26] Stefanos Gkikas and Manolis Tsiknakis. 2024. Twins-PainViT: Towards a Modality-Agnostic Vision Transformer Framework for Multimodal Automatic Pain Assessment Using Facial Videos and fNIRS. In *2024 12th International Conference on Affective Computing and Intelligent Interaction Workshops and Demos (ACIIW)*. 13–21. <https://doi.org/10.1109/ACIIW63320.2024.00007>

[27] Noemi Gozzi, Greta Pretoni, Federico Ciotti, Michèle Hubli, Petra Schweinhardt, Armin Curt, and Stanisa Raspovic. 2024. Unraveling the physiological and psychosocial signatures of pain by machine learning. *Med* 5, 12 (2024), 1495–1509.

[28] Keela Herr, Patrick J. Coyne, Tonya Key, Renee Manworren, Margo McCaffery, Sandra Merkel, Jane Pelosi-Kelly, and Lori Wild. 2006. Pain Assessment in the Nonverbal Patient: Position Statement with Clinical Practice Recommendations. *Pain Management Nursing* 7, 2 (2006), 44–52. <https://doi.org/10.1016/j.pmn.2006.02.003>

[29] Dong Huang, Xiaoyi Feng, Haixi Zhang, Zitong Yu, Jinye Peng, Guoying Zhao, and Zhaoqiang Xia. 2022. Spatio-Temporal Pain Estimation Network With Measuring Pseudo Heart Rate Gain. *IEEE Transactions on Multimedia* 24 (2022), 3300–3313. <https://doi.org/10.1109/TMM.2021.3096080>

[30] Xinwei Ji, Tiamming Zhao, Wei Li, and Albert Zomaya. 2023. Automatic Pain Assessment with Ultra-short Electrodermal Activity Signal. In *Proceedings of the 38th ACM/SIGAPP Symposium on Applied Computing* (Tallinn, Estonia) (SAC '23). Association for Computing Machinery, New York, NY, USA, 618–625. <https://doi.org/10.1145/3555776.3577721>

[31] Mingzhe Jiang, Yufei Li, Jiangshan He, Yuqiang Yang, Hui Xie, and Xueli Chen. 2024. Physiological Time-series Fusion with Hybrid Attention for Adaptive Recognition of Pain. *IEEE Journal of Biomedical and Health Informatics* (2024), 1–9. <https://doi.org/10.1109/JBHI.2024.3456441>

[32] Mingzhe Jiang, Riitta Rosio, Sanna Salanterä, Amir M. Rahmani, Pasi Liljeberg, Daniel S. da Silva, Victor Hugo C. de Albuquerque, and Wanqing Wu. 2024. Personalized and adaptive neural networks for pain detection from multi-modal physiological features. *Expert Systems with Applications* 235 (2024), 121082. <https://doi.org/10.1016/j.eswa.2023.121082>

[33] Lucille A Joel. 1999. The fifth vital sign: pain. *AJN The American Journal of Nursing* 99, 2 (1999), 9.

[34] Mohammad Kachuee, Shayan Fazeli, and Majid Sarrafzadeh. 2018. ECG Heartbeat Classification: A Deep Transferable Representation. In *2018 IEEE International Conference on Healthcare Informatics (ICHI)*. 443–444. <https://doi.org/10.1109/ICHI.2018.00092>

[35] Joanna G Katzman and Rollin Mac Gallagher. 2024. Pain: The Silent Public Health Epidemic. *Journal of Primary Care & Community Health* 15 (2024), 21501319241253547.

[36] Alan David Kaye, Mark R Jones, Adam M Kaye, Juan G Ripoll, Vincent Galan, Burton D Beakley, Francisco Calixto, Jamie L Bolden, Richard D Urman, and Laxmaiah Manchikanti. 2017. Prescription opioid abuse in chronic pain: an updated review of opioid abuse predictors and strategies to curb opioid abuse: part 1. *Pain physician* 20, 2 (2017), S93.

[37] Muhammad Umar Khan, Sumair Aziz, Luke Murtagh, Girija Chetty, Roland Goecke, and Raul Fernandez Rojas. 2025. Empirically Transformed Energy Patterns: A novel approach for capturing fNIRS signal dynamics in pain assessment. *Computers in Biology and Medicine* 192 (2025), 110300. <https://doi.org/10.1016/j.combiomed.2025.110300>

[38] Muhammad Umar Khan, Girija Chetty, Roland Goecke, and Raul Fernandez-Rojas. 2025. A Systematic Review of Multimodal Signal Fusion for Acute Pain Assessment Systems. *ACM Comput. Surv.* (2025). <https://doi.org/10.1145/3737281>

[39] Muhammad Umar Khan, Maryam Sousani, Niraj Hirachan, Calvin Joseph, Maryam Ghahramani, Girija Chetty, Roland Goecke, and Raul Fernandez-Rojas. 2024. Multilevel Pain Assessment with Functional Near-Infrared Spectroscopy: Evaluating  $\Delta\text{HbO}_2$  and  $\Delta\text{HHb}$  Measures for Comprehensive Analysis. *Sensors* 24, 2 (2024). <https://doi.org/10.3390/s24020458>

[40] Younghun Kong and Ki H. Chon. 2024. Electrodermal activity in pain assessment and its clinical applications. *Applied Physics Reviews* 11, 3 (08 2024), 031316. <https://doi.org/10.1063/5.0200395>

[41] JiaHao Li, JinCheng Luo, YanSheng Wang, YunXiang Jiang, Xu Chen, and YuJuan Quan. 2025. Automatic Pain Assessment Based on Physiological Signals: Application of Multi-Scale Networks and Cross-Attention Cross-Attention. In *Proceedings of the 2024 13th International Conference on Bioinformatics and Biomedical Science (ICBBS '24)*. Association for Computing Machinery, New York, NY, USA, 113–122. <https://doi.org/10.1145/3704198.3704212>

[42] Zhenyuan Lu, Burcu Ozek, and Sagar Kamarthi. 2023. Transformer encoder with multiscale deep learning for pain classification using physiological signals. *Frontiers in Physiology* 14 (2023). <https://doi.org/10.3389/fphys.2023.1294577>

[43] Serge Marchand. 2024. *The pain phenomenon*. Vol. 13. Springer Nature.

[44] DA Meehan, ME McRae, DA Rourke, C Eisenring, and FA Imperial. 1995. Analgesic administration, pain intensity, and patient satisfaction in cardiac surgical patients. *American Journal of Critical Care* 4, 6 (1995), 435–442.

[45] Minh-Duc Nguyen, Hyung-Jeong Yang, Soo-Hyung Kim, Ji-Eun Shin, and Seung-Woo Kim. 2024. Transformer with Leveraged Masked Autoencoder for video-based Pain Assessment. arXiv:2409.05088 [cs.CV]

[46] Manisha S. Patil and Hitendra D. Patil. 2024. Ensemble Neural Networks for Multimodal Acute Pain Intensity Evaluation using Video and Physiological Signals. *Journal of Computational Analysis and Applications (JoCAA)* 33, 05 (Sep. 2024), 779–791.

[47] Elisavet Pavlidou and Manolis Tsiknakis. 2025. Multimodal Pain Assessment Based on Physiological Biosignals: The Impact of Demographic Factors on Perception and Sensitivity. In *Proceedings of the 11th International Conference on Information and Communication Technologies for Ageing Well and e-Health - ICT4AWE*. INSTICC, SciTePress, 320–329. <https://doi.org/10.5220/0013426800003938>

[48] Kim Ngan Phan, Ngumimi Karen Iyortsuun, Sudarshan Pant, Hyung-Jeong Yang, and Soo-Hyung Kim. 2023. Pain Recognition With Physiological Signals Using Multi-Level Context Information. *IEEE Access* 11 (2023), 20114–20127. <https://doi.org/10.1109/ACCESS.2023.3248654>

[49] Pooja Prajod, Dominik Schiller, Dakitha Withanage Don, and Elisabeth André. 2024. Faces of Experimental Pain: Transferability of Deep-Learned Heat Pain Features to Electrical Pain\*. In *2024 12th International Conference on Affective Computing and Intelligent Interaction Workshops and Demos (ACIIW)*. 31–38. <https://doi.org/10.1109/ACIIW63320.2024.00009>

[50] Kathleen A Puntillo, Daphne Stannard, Christine Miaskowski, Karen Kehrle, and Sheila Gleeson. 2002. Use of a pain assessment and intervention notation (P.A.I.N.) tool in critical care nursing practice: Nurses' evaluations. *Heart & Lung* 31, 4 (2002), 303–314. <https://doi.org/10.1067/mhl.2002.125652>

- [51] Carlos Riquelme, Joan Puigcerver, Basil Mustafa, Maxim Neumann, Rodolphe Jenatton, André Susano Pinto, Daniel Keysers, and Neil Housley. 2021. Scaling vision with sparse mixture of experts. *Advances in Neural Information Processing Systems* 34 (2021), 8583–8595.
- [52] Raul Fernandez Rojas, Xu Huang, and Keng-Liang Ou. 2016. Region of Interest Detection and Evaluation in Functional near Infrared Spectroscopy. *Journal of Near Infrared Spectroscopy* 24, 4 (2016), 317–326. <https://doi.org/10.1255/jnirs.1239>
- [53] Raul Fernandez Rojas, Julio Romero, Jehu Lopez-Aparicio, and Keng-Liang Ou. 2021. Pain Assessment based on fNIRS using Bi-LSTM RNNs. In *2021 10th International IEEE/EMBS Conference on Neural Engineering (NER)*. 399–402. <https://doi.org/10.1109/NER49283.2021.9441384>
- [54] Riccardo Sabbadini, Giulia Di Tomaso, Massimiliano Carassiti, and Giuseppe Francesco Italiano. 2024. The need of raw physiological data for more comprehensive pain studies. *AI & SOCIETY* (2024), 1–8.
- [55] Riccardo Sabbadini, Carlo Massaroni, Joshua Di Tocco, Emiliano Schena, Domenico Formica, Alessia Mattei, Rita Cataldo, Francesca Gargano, and Massimiliano Carassiti. 2020. A non-invasive system for epidural space detection: comparison with Compuflo. In *2020 IEEE International Workshop on Metrology for Industry 4.0 & IoT*. 304–308. <https://doi.org/10.1109/MetroInd4.0IoT48571.2020.9138230>
- [56] Vivian Santiago. 2022. Painful Truth: The Need to Re-Center Chronic Pain on the Functional Role of Pain. *Journal of Pain Research* 15 (2022), 497–512. <https://doi.org/10.2147/JPR.S347780>
- [57] Argyrios Stampas, Claudia Pedroza, Jennifer N Bush, Adam R Ferguson, John L Kipling Kramer, and Michelle Hook. 2020. The first 24 h: opioid administration in people with spinal cord injury and neurologic recovery. *Spinal Cord* 58, 10 (2020), 1080–1089.
- [58] Marie-Hélène Tessier, Jean-Philippe Mazet, Elliot Gagner, Audrey Marcoux, and Philip L Jackson. 2024. Facial representations of complex affective states combining pain and a negative emotion. *Scientific Reports* 14, 1 (2024), 11686.
- [59] Patrick Thiam, Peter Bellmann, Hans A. Kestler, and Friedhelm Schwenker. 2019. Exploring deep physiological models for nociceptive pain recognition. *Sensors* 19 (10 2019), 4503. Issue 20. <https://doi.org/10.3390/s19204503>
- [60] Jo Vianto, Anjitha Divakaran, Hyunjeong Yang, Soonja Yeom, Seungwon Kim, Soohyung Kim, and Jieun Shin. 2025. Multimodal Model for Automated Pain Assessment: Leveraging Video and fNIRS. *Applied Sciences* 15, 9 (2025). <https://doi.org/10.3390/app15095151>
- [61] Philipp Werner, Ayoub Al-Hamadi, Robert Niese, Steffen Walter, Sascha Gruss, and Harald C. Traue. 2014. Automatic Pain Recognition from Video and Biomedical Signals. In *2014 22nd International Conference on Pattern Recognition*. 4582–4587. <https://doi.org/10.1109/ICPR.2014.784>
- [62] Ruicong Zhi and Junwei Yu. 2019. Multi-modal Fusion Based Automatic Pain Assessment. In *2019 IEEE 8th Joint International Information Technology and Artificial Intelligence Conference (ITAIC)*. 1378–1382. <https://doi.org/10.1109/ITAIC.2019.8785727>